Talanta 85 (2011) 770–778

Contents lists available at ScienceDirect

Talanta

journal homepage: www.elsevier.com/locate/talanta

Electrochemical analysis of HIV-1 reverse transcriptase serum level: Exploiting protein binding to a functionalized nanostructured surface

Mahmoud Labib, Sanela Martić, Patrick O. Shipman, Heinz-Bernhard Kraatz*

Department of Chemistry, University of Western Ontario, 1151 Richmond Street, London, ON, Canada N6A 5B7

ARTICLE INFO

Article history:
Received 17 March 2011
Received in revised form 26 April 2011
Accepted 27 April 2011
Available online 5 May 2011

Keywords:
HIV-1 reverse transcriptase
Ferrocene
Square wave voltammetry
Bioorganometallics
Nanogold

ABSTRACT

This manuscript describes an electrochemical approach to the detection of the reverse transcriptase of the human immunodeficiency virus type-1 (HIV-1 RT) in serum exploiting an organometallic peptide conjugate that is chemically linked to a nanostructured gold surface. The assay format is based on the formation of a thin film of a ferrocene-labeled lipoic acid (Fc-LA) onto a gold nanoparticles-functionalized screen-printed carbon electrode (GNPs-SPCE). Time-of-Flight secondary ion mass spectrometry (TOF-SIMS) and X-ray photoelectron spectroscopy were employed to confirm the binding of the Fc-LA to the electrode surface via formation of a gold–thiol bond. The RT biosensor was developed by covalent attachment of the peptide VEAIIRILQQLLFIH to the carboxylic acid group of Fc-LA. Square wave voltammetry offered a two-dimensional measurement of RT based on the anodic shift and reduction of current density of the Fc redox signal upon binding of RT to its specific peptide. This allowed a linear quantification of the target RT in the range of 1–500 pg mL^{-1} equivalent to 0.9–427 fM, with a detection limit of 0.8 pg mL^{-1} (0.7 fM) with a short response time.

1. Introduction

Since its first recognition in 1981, a large number of direct and indirect methods have been developed for human immunodeficiency virus (HIV) detection [1]. These methods include the detection of HIV type 1 (HIV-1) or HIV type 2 (HIV-2) antibodies [2], viral RNA [3] and viral P24 assays [4], viral load analysis [5], and CD4+ T lymphocytes counting [6]. However, antibody-based assays are temporarily used as the gold standard for laboratory diagnosis of HIV infection, whereas the viral load analysis and CD4+ T lymphocyte counting are used to evaluate the progression of infection and the effectiveness of the antiviral therapy [7]. Compared to antibody-based assays, RNA assay is not recommended in clinical practice due to the potential false positives from polymerase chain reaction (PCR)-based assays. Additionally, the high cost of nucleic acid-based testing strategies, together with the significant technical demands required for their delivery, has precluded their use in resource-limited settings (RLS) [8]. In the same context, viral P24 assays are less trustworthy due to the variability of the P24 antigen results for a given viral RNA load. Furthermore, the presence of P24-specific antibodies in serum may cause under-estimation or give false-negative results [9]. Although the current application of antibody-based assays is not replaceable in clinical practice, it should be stressed that there are circumstances where these assays are less trustworthy. This includes viral infections associated with viruses having weak antigenic or hypermutable features which can substantially minimize or eliminate certain antigenic characteristics resulting in neutralization escape or in low level of antibody titer in the host serum [10]. Additionally, there is a quite long lag period between the infection and the appearance of enough antibodies to be detected by conventional ELISA or Western blot assays [11].

In contrast to immunoassays in which the antibodies need a long period to generate, detection of HIV enzymes presents an alternative strategy for early diagnosis of the infection. Furthermore, it does not suffer from the disadvantages of other HIV detection methodologies [12–14]. HIV-1 reverse transcriptase (RT), one of three enzymes encoded by the HIV genome is an asymmetric dimer of 66-kDa subunit (p66) and a 51-kDa subunit (p51). RT catalyzes the conversion of the viral genome from a single-stranded RNA into a double-stranded DNA in a relatively complex process. This reverse transcription is entirely catalyzed by RT using its two catalytic activities, including the DNA-polymerase activity which can copy either a DNA or an RNA template into DNA, and the ribonuclease H activity which concurrently cleaves the RNA strand in the DNA–RNA heteroduplex formed [15]. The absolute requirement of RT activity for HIV replication has made this enzyme one of the major targets for detection of HIV. Currently, several techniques have been adopted for RT detection, including PCR [16], electrophoresis [17], combined microbalance array and mass spectrometry [18],

* Corresponding author. Tel.: +1 519 661 2166x81561; fax: +1 519 661 3022.
E-mail address: hkraatz@uwo.ca (H.-B. Kraatz).

0039-9140/$ – see front matter © 2011 Elsevier B.V. All rights reserved.
doi:10.1016/j.talanta.2011.04.070

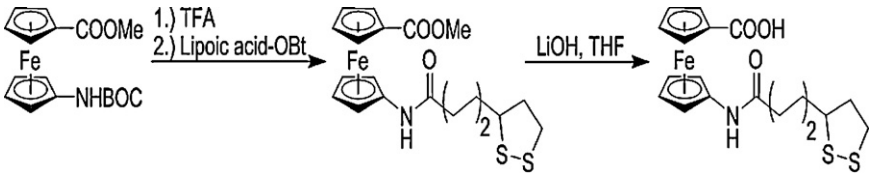

Scheme 1. The synthesis route for the ferrocene-labeled lipoic acid.

and fluorescence techniques [19]. However, there is an ongoing need for rapid analytics for viral enzymes that are sensitive, cheap, robust, simple to use, and limited-to-no sample preparation. In this context, recent reports have shown the ability of electrochemical sensors to detect several biomolecules, including proteins [20–25], glycoproteins [26], and carbohydrates [27,28], with high sensitivity and excellent reproducibility.

Here, we describe the preparation of a thin film of a ferrocene-labeled lipoic acid (Fc-LA) derivative (see Scheme 1) on a screen-printed carbon electrode functionalized with gold nanoparticles (GNPs-SPCE), which is then modified with short peptide VEAIIRILQQLLFIH, reported earlier by Gleenberg et al. [29] to bind to the reverse transcriptase of HIV-I. This modified electrode is then used to detect HIV-1 RT in human serum by square-wave voltammetry. In this report, we provide details of the analytical parameter, including the dynamic range, detection limit, selectivity, and reproducibility.

2. Experimental

2.1. Materials and reagents

Screen-printed electrodes on ceramic substrate (L33 mm × W10 mm × H0.5 mm) were purchased from Dropsens (Oviedo, Spain). HIV-1 reverse transcriptase (RT) enzyme was purchased from Applied Biosystems (Streetsville, ON, Canada). The RT-specific peptide (VEAIIRILQQLLFIH) was purchased from Bio Basic Inc. (Markham, ON, Canada). HIV-1 integrase was purchased from ProSpecBio (USA). HIV-1 protease was obtained from Anaspec (CA, USA). Human serum from male AB plasma, HIV-1 protease-specific peptide (VVStaASta or pepstatin), *N*-(3-Dimethylaminopropyl)-*N*′-ethyl-carbodiimide hydrochloride (EDC), *N*-Hydroxysuccinimide (NHS), 3-(*N*-morpholino) propanesulfonic acid (MOPS), and *O*-(2-mercaptoethyl)-*O*′-methyl-hexa(ethylene glycol) were purchased from Sigma–Aldrich (Canada). All other reagents were of analytical grade. Deionized water (18.2 MΩ cm resistivity) from a Millipore Milli-Q system was used throughout this work. Full synthetic details for the preparation of Fc-LA, including its ^{1}H NMR and ^{13}C NMR spectra, are provided in the Supplementary data.

2.2. Preparation of the peptide-modified electrode

Prior to experiments, the screen-printed electrode was washed thoroughly with deionized water then dried with N_2. The self-assembly of the Fc-LA on the electrode surface was performed by incubating the working electrode spot with 2 mM of Fc-LA in basic water (5 μL) in a humidity chamber for 24 h, at room temperature. After rinsing with deionized water, the working electrode was incubated with 1:1 mixture of EDC and NHS (10 mM) for 5 h, at room temperature. Afterwards, the working electrode was incubated with 1 mM of the RT-specific peptide in 10 mM sodium phosphate buffer, pH 7, overnight at 4 °C. Subsequently, the peptide-modified electrode was incubated with 1.0 mM aqueous solution of *O*-(2-mercaptoethyl)-*O*′-methyl-hexa(ethylene glycol) for 5 min to back-fill the empty spots of the electrode surface. Finally, the electrode was rinsed with deionized water and dried with N_2 to give the peptide-modified sensor surface.

2.3. X-ray photoelectron spectroscopy (XPS)

XPS was employed to characterize the sensor surface after the self-assembly of the Fc-LA onto the GNPs-SPCE. The XPS spectra were acquired using an Axis Ultra spectrometer (Kratos Analytical, UK) with a monochromatic Al-Kα X-ray source (15 mA, 14 kV). The takeoff angle between the film surface and the photoelectron energy analyzer was 90°. A typical operating pressure was around 5×10^{-10} Torr in the analysis chamber. Survey spectra (0–1100 eV) were taken at constant analyzer pass energy of 160 eV and were applied on an analysis area of 300 μm × 700 μm. High-resolution analyses were carried out at a pass energy of 20 eV on the same surface area. The binding energies were referenced to Au $4f_{7/2}$ at 83.96 eV and the spectrometer dispersion was adjusted to give a binding energy of 932.62 eV for the Cu $2p_{3/2}$ line of metallic copper. Acquired spectra were charge-corrected to the main line of the C 1s spectrum (adventitious carbon) set at 284.8 eV and analyzed using CasaXPS software (version 2.3.14).

2.4. Time-of-Flight secondary ion mass spectrometry (TOF-SIMS)

TOF-SIMS was employed to characterize the sensor surface after the covalent coupling of the RT-specific peptide to the carboxylic acid group of the Fc-LA. TOF-SIMS experiments were performed using TOF-SIMS IV (ION-TOF GmbH, Münster, Germany), which was equipped with a Bi liquid metal ion source. For all measurements, a 25 keV Bi_3^+ cluster primary ion beam with a pulse width of 12 ns (target current of ~1.0 pA) was utilized. The cycle time for the bombardment processes and detection was 100 μs (or 10 kHz). A pulsed, low energy electron flood was used to neutralize the sample charging. For each sample, spectra were collected from 128 × 128 pixels over an area of 500 μm × 500 μm for 60 s. Positive and negative ion spectra were internally calibrated by using H^+, H_2^+, CH_3^+, H^-, C^-, and CH^- signals, respectively. Two spots per sample were analyzed by using a random approach. Spectra were analyzed using IonSpec Application, version 4.1.0.1 (ION-TOF GmbH, Germany).

2.5. Electrochemical measurements

All electrochemical studies, including cyclic voltammetry (CV), square wave voltammetry (SWV), and electrochemical impedance spectroscopy (EIS) were performed with an electrochemical analyzer (CH Instruments 660B, TX, USA) connected to a personal computer. All measurements were carried out at room temperature in an enclosed and grounded Faraday cage. A conventional three-electrode configuration printed on a ceramic substrate, including a gold nanoparticles/carbon electrode as the working electrode (0.126 cm^2), a carbon counter electrode, and a silver pseudo-reference electrode. A three-electric contacts edge connector was used to connect the screen-printed electrode with the potentiostat (Dropsens, Oviedo, Spain). The open-circuit or rest potential of the system was measured prior to all electrochemical experiments to prevent sudden potential-related changes in the SAM. CV and SWV

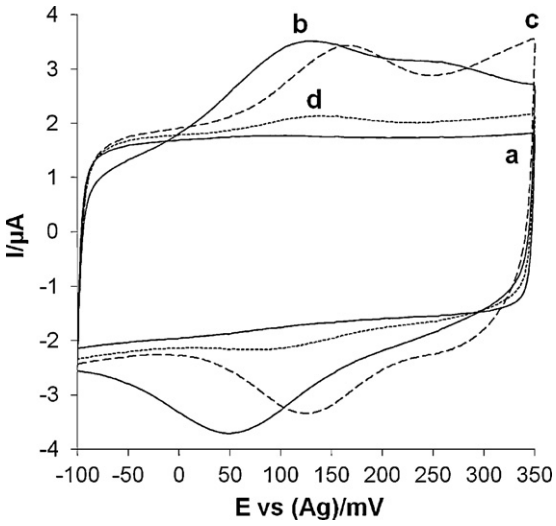

Fig. 1. Cyclic voltammograms of the RT biosensor after each immobilization or binding step. CVs were recorded at a scan rate of 100 mV s^{-1}, in the same buffer where (a) bare GNPs-SPCE; (b) after coating with Fc-LA; (c) after covalent coupling of the RT-specific peptide; and (d) after surface back-filling with the diluent.

experiments were started from the rest potential in 10 mM sodium phosphate buffer, pH 7. CV experiments were performed at a scan rate of 100 mV s^{-1} in the potential range from −100 to 350 mV. SWV experiments were carried out in the range from −100 to 300 mV with a step potential of 5 mV, amplitude of 25 mV, and frequency of 10 Hz. EIS experiments were performed in 10 mM sodium phosphate buffer (pH 7), containing 1.0 mM $[Fe(CN)_6]^{3-/4-}$ as a redox probe. EIS measurements were conducted in the frequency range of 100 kHz to 0.1 Hz, at a formal potential of 250 mV and AC amplitude of 5 mV. Importantly, all measurements were repeated for a minimum of three times with separate electrodes to obtain statistically meaningful results.

3. Results and discussion

3.1. Electrochemical characteristics of the developed biosensor

The electrochemical characteristics of the fabricated biosensor were investigated by cyclic voltammetry (CV) in 10 mM sodium phosphate buffer at pH 7 and, as is expected for a thin film of surface-bound molecules, it displays a linear current response as a function of scan rate [30] (see Supplemental Information). As shown in Fig. 1, the CV scan of the pre-treatment electrode surface did not show any Faradaic signal and displays charging current only (*curve a)*. Upon formation of a film of Fc-LA, a redox signal appears due to the redox of the ferrocene group (*curve b*). Generally, Fc groups embedded in alkyl monolayers give rise to broad CV signal [31]. Covalent coupling of the RT-specific peptide to the carboxylic acid-terminated Fc-LA led to a reduction of the current response (*curve c*), presumably due to a lack of penetration of solvent and ions into the film. Next, back-filling with *O*-(2-mercaptoethyl)-*O*′-methyl-hexa(ethylene glycol) greatly reduced the redox currents by blocking the access of conducting ions further (*curve d*). We also considered the estimation of the electro-active area of the GNPs-SPCE working electrode using Randles-Sevčik Eq. (1) for quasi-reversible electron transfer processes [32]

$$I_p = 2.69 \times 10^5 n^{3/2} v^{1/2} D^{1/2} AC \quad (1)$$

where n is the number of electrons participating in the redox process, v is the scan rate, A is the area of the electrode, C is the concentration of the probe molecule in mol cm^{-3}, and D is the diffusion coefficient for 1.0 mM potassium ferrocyanide in 1.0 M KCl (6.3×10^{-6} cm^2 s^{-1}). Subsequently, an active area of 0.009 cm^2 was calculated. The electrochemical properties of the sensing interface following each modification step are presented in Table 1. A nonzero peak-to-peak separation, ΔE, may be a result of a variety of factors such as solvation and lateral interactions between the redox moieties [33]. The peak full width at half maximum, ΔE_{fwhm}, can be used to evaluate the organizational behavior of films. In well-ordered systems with minimal interactions between the redox centers, ΔE_{fwhm} should be 90.6 mV at 25 °C [34]. Relatively higher value for ΔE_{fwhm} (∼130) was observed after the formation of the SAM of Fc-LA, suggesting some inhomogeneity of the Fc environment and the existence of repulsive interactions between the redox centers [35]. However, coupling of the RT-specific peptide to the Fc-LA and surface back-filling might have led to a more uniform surface packing with reduced electrostatic repulsion, evidenced by the ΔE_{fwhm} values close to 90 mV [36]. The ratio of the anodic and cathodic peak currents, I_{pa}/I_{pc}, was close to unity, indicating a reversible redox process. The Faradic charge associated with the Fc/Fc^+ electron-transfer processes was determined by integrating the cathodic peak area of the CVs from which the surface concentration (Γ_{Fc}) was calculated, according to Eq. (2)

$$\Gamma_{Fc} = \frac{Q}{nFA} \quad (2)$$

where Γ_{Fc} is the surface concentration associated with the redox activity, Q is the surface charge, n is the number of electrons ($n = 1$ for Fc), F is Faraday's constant, and A is the area of the electrode [34]. After the self-assembly of the Fc-LA on the electrode surface, the sensor displayed a surface probe density of $11.8 \pm 0.4 \times 10^{-10}$ mol cm^{-2} which indicates good packing of the Fc-LA on the sensor surface [37].

3.2. XPS studies

The XPS survey scan of Fc-LA modified GNP-SPCE reveals the presence of five intense peaks centred at 707.5, 531.8, 284.7, 163.6, and 83.8 eV, which were assigned to Fe 2p, O 1s, C 1s, S 2p and Au 4f excitations, respectively (Fig. 2a). The Fe core level signals provide further evidence for the adsorption of the Fc-LA on the electrode surface (Fig. 2b). In the Fe 2p XPS, the Fe $2p_{3/2}$ level was deconvoluted into two peaks at 707.93 eV and 706.36 eV, where the former peak is characteristic for Fe(II) in the Fc-LA. This clearly confirms the presence of the Fc moiety on the electrode surface [38,39]. The sulfur signal is of interest because it forms the basis of the Au-S bond formation. In this context, fitting of the S 2p spectra gave two triplets, each with an area ratio of 8:1:1 (Fig. 2c). The S $2p_{3/2}$ peak corresponds to the S atoms bound to the gold surface as thiolate species, whereas the S $2p_{1/2}$ indicates a physisorbed moiety [40,41].

Table 1
Electrochemical properties of the developed biosensor using the nanogold functionalized screen printed electrode (E°, ΔE and ΔE_{fwhm} in mV, and Γ_{Fc} in $\times 10^{-10}$ mol cm^{-2}) and the values are taken from CV data.

	E°	ΔE	ΔE_{fwhm}	I_{pa}/I_{pc}	Γ_{Fc}
After Fc-labeled SAM formation	84.28 ± 4.42	59.95 ± 0.98	130.05 ± 5.02	1.08 ± 0.09	11.8 ± 0.4
After RT-specific peptide binding	143.55 ± 3.46	31.7 ± 1.5	97.1 ± 1.96	1 ± 0.01	6.76 ± 0.06
After surface back-filling	118.23 ± 1.24	35.05 ± 2.48	95.8 ± 3.35	1 ± 0.03	1.25 ± 0.35

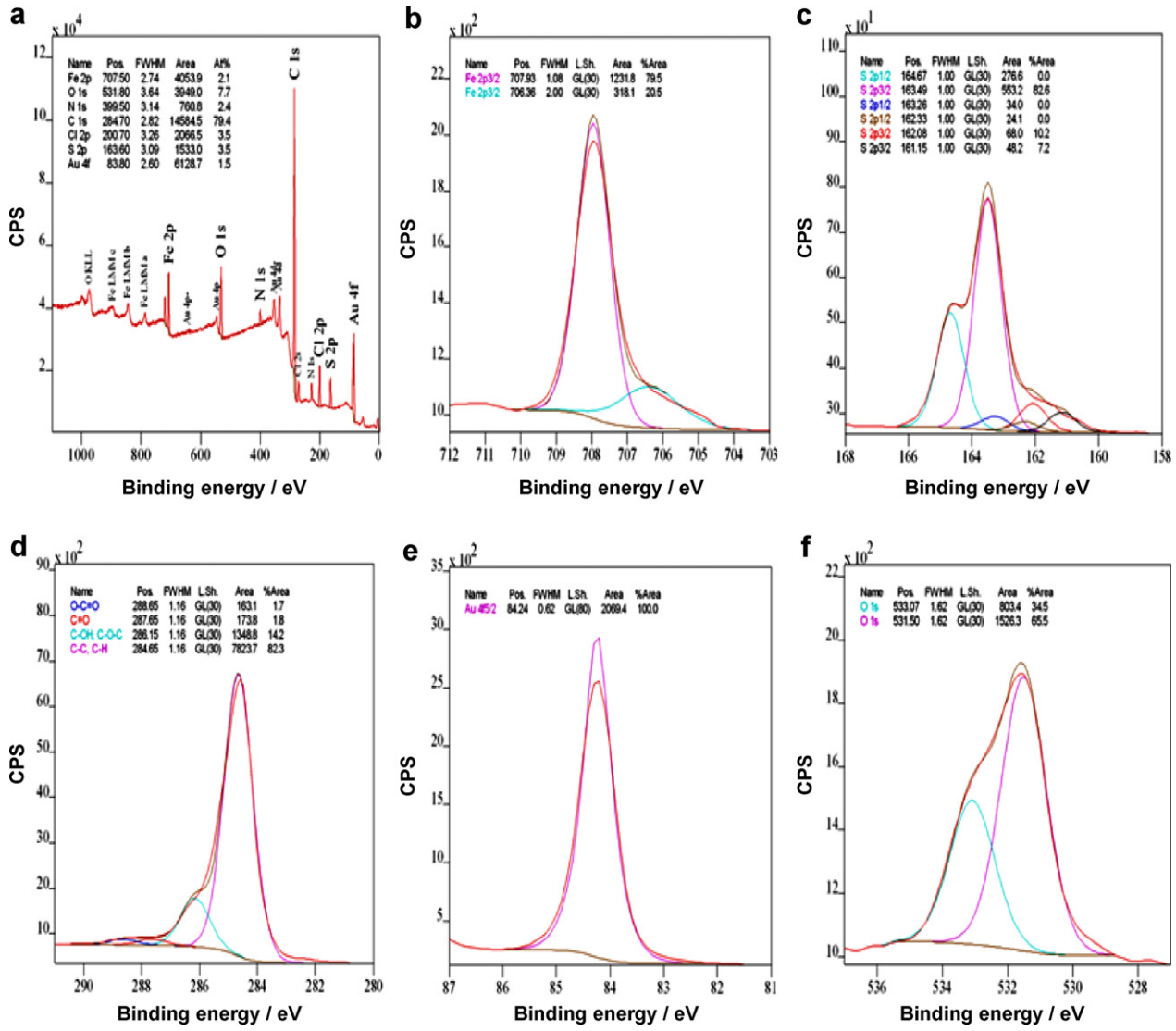

Fig. 2. X-ray photoelectron spectroscopy (XPS) of the Fc-LA modified GNPs-SPCE surface. (a) Survey scan of the film covering the electrode surface. High resolution XPS core level spectra of (b) iron, (c) sulfur, (d) carbon, (e) gold, and (f) oxygen.

Unlike the XPS spectra of sputtering gold electrodes [21,22], GNPs-SPCE is characterized by predominant C peaks, including C 1s, C2s, and C 2p levels due to the nature of the graphite matrix. XPS survey scan also revealed the presence of an asymmetrical C 1s peak with a full width at half maximum (FWHM) of 2.82 eV. This could be attributed to contributions from partially oxidized surface species, polymeric binder, and organic contaminants, which is generally expected for graphitic surfaces [42–44]. The GNPs-SPCE surface contains a major fraction of native carbon peak located at 284.65 eV, which could be attributed to sp^2 hybridized C–C bonds in graphite as well as C–H bonds [45]. The surface also contains minor fractions of C–O and C–N (286.15 eV), C═O (287.65 eV), and O–C═O (288.65 eV), as shown in Fig. 2d. The results are in agreement with the reported peaks on classical carbon surface [46,47]. The Au 4f spectrum exhibited a peak at 84.24 eV, which is characteristic to GNPs containing surfaces [48]. As shown in Fig. 2e, two peaks of Au^0 were observed at 87.7 eV and 84.21 eV, respectively. The O 1s spectrum was deconvoluted into two peaks, at 533.07 eV due to the double bonded oxygen (C═O), and at 531.5 eV due to the single bonded oxygen (OH/C–O) [49], as shown in Fig. 2f.

Notably, the ratio of XPS core level intensities of Au 4f to C1s, I_{Au}/I_C, can be used to estimate the amount of the GNPs on the SPCE surface [50]. The calculated I_{Au}/I_C value is 0.42. Based on the previous electrochemical study (Section 3.1), the amount of GNPs on the surface also can be estimated from the ratio of the electro-active surface area to the geometrical surface area. In such case, a value of 0.1 was estimated. This variation might be attributed to the presence of the polymeric binder covering the GNPs-SPCE surface, which could act as an insulating layer, increasing the activation barrier for the electron transfer and causing a limitation of the electron transfer rate at the electrode/electrolyte interface [51]. Other factors should be taken into consideration, including the amount or loading of graphite, functionalization of graphite, wetability of the electrode surface (hydrophilic *vs.* hydrophobic), and curing regime [52–54]. Furthermore, a degree of structural reorganization accompanying the redox reaction cannot be neglected. Eventually, a more accurate I_{Au}/I_C value was provided by XPS. Notably, many authors indicated the necessity of SPCE pre-treatment, with acids [55], alkali [56], plasma [57], or preanodization [58,59], before electro-active surface area estimation. However, this was not attempted in our study which aims at the development of a simple miniaturized point of care (POC) for rapid detection of HIV enzymes based on disposable GNPs-SPCEs.

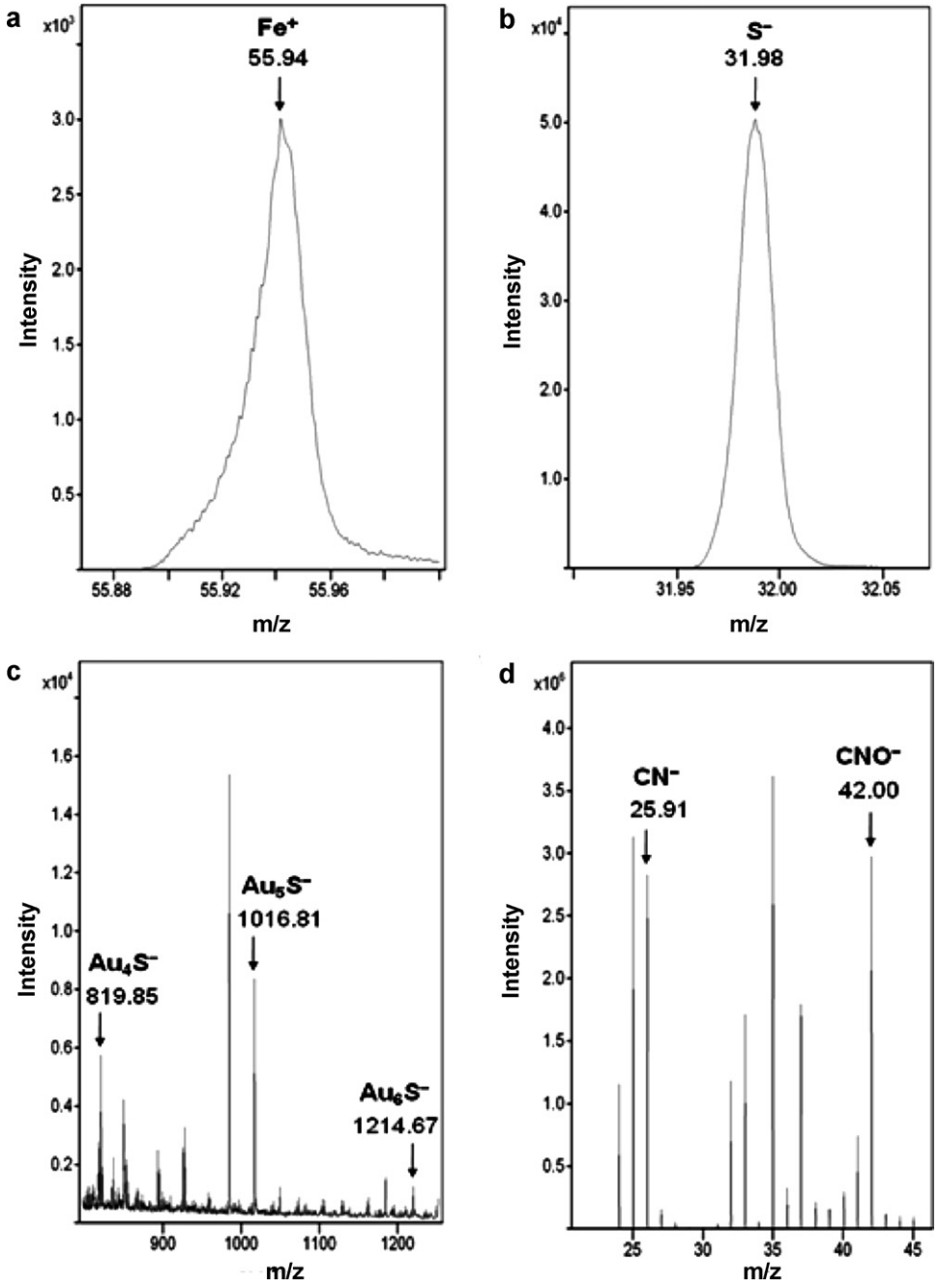

Fig. 3. TOF-SIMS spectra of the developed RT biosensor, showing (a) Fe^+ in the positive mode and (b) S^-; (c) Au_4S^-, Au_5S^-, and Au_6S^-; (d) CN^- and CNO^- fragment ion intensities in the negative mode.

3.3. TOF-SIMS results

TOF-SIMS, a highly useful technique for speciation of surface attached chemical groups [60], confirmed the formation of the Fc-LA film on the gold surface, evidenced by the Fe^+ peak in the positive ion mode (Fig. 3a) and the S^- peak (Fig. 3b), Au_4S^-, Au_5S^-, and Au_6S^- cluster peaks in the negative ion mode (Fig. 3c). After attachment of the RT-specific peptide, the TOF-SIMS exhibited signals due to CN^- and CNO^-, presumably formed by the decomposition of the peptide under TOF-SIMS conditions (Fig. 3d). The TOF-SIMS analysis of amino acid fragments was performed in order to identify the key backbone (C–N) cleavage ions. Although the molecular ion peaks were not observed, the selected experimental fragment ions compare well with the theoretical *m/z* values as presented in Table 2.

3.4. Surface characterization via scanning electron microscopy

Scanning electron microscopy (SEM) images were obtained using LEO 1540XB FIB/SEM model (Zeiss, Germany), with an acceleration voltage of 1.0 kV and a magnification power of 50 kX. Fig. 4a depicts the typical SEM image of the bare GNPs-SPCE which shows bright granular clusters of GNPs embedded in a flake-like graphite matrix covered with a polymeric binder [61]. Upon coupling of the RT-specific peptide to the SAM of Fc-LA preformed on the electrode

Table 2
Negative cleavage ions for peptide and Fc-peptide backbones and the proposed cleaving sites (theoretical peptide fragments were calculated using the Protein Prospector, UCSF mass spectrometry facility).

Ion species	*m/z*	
	Experimental	Theoretical
1	300.89	300.10
2	413.01	413.22
3	911.28	911.52
4	911.11	911.62
5	783.03	783.51
6	655.13	655.42
7	429.39	429.32
8	715.28	715.19
9	911.28	911.61
10	783.03	783.52
11	655.15	655.42
12	429.39	429.32

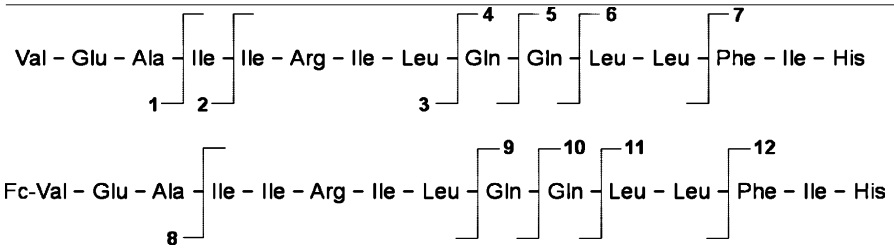

surface, a smooth denser layer of the peptide was formed, covering the rough GNPs surface [62] (Fig. 4b).

3.5. RT analysis

RT analysis was performed by incubating the biosensor with aliquots of RT-spiked human serum in 25 mM MOPS (pH 7.2), containing 100 mM NaCl and 7.5 mM $MnCl_2$, for 1 h at 37 °C. A concentration-dependant response for RT was measured by square wave voltammetry (SWV). The linker between the GNP and the Fc group is an important part of the system in acting as a potential conduit for electron transfer [63]. Modulation of the redox signal can be caused by changes in the ability of the redox probe to access the electrode surface, thereby changing the electron transfer kinetics of the system [64–66], or a partial encapsulates of the Fc label upon binding of RT to the conjugate preventing efficient access of counter ions to the Fc group [67]. SWV was adopted for RT analysis as an effective and rapid technique with well-established advantages, including low detection limits and good discrimination against background currents [68]. Fig. 5 shows a series of SWVs of the sensor surface as a function of increasing RT concentrations. As shown in Fig. 5a, binding of RT to the surface-bound Fc-peptide conjugate resulted in a shift to higher potential while the current intensity decreased. Such anodic shifts indicate that the Fc becomes more difficult to oxidize once RT is bound to the conjugate. Hence, the modulation of the electrochemical signal was recorded as a function of the changes in intensity of the Fc current signals (ΔI) and anodic shifts in the peak potential (ΔE). As shown in Fig. 5b and c, ΔE *vs.* enzyme concentration was linear in the range from 1 to 500 pg mL^{-1}, equivalent to 8.6–427.4 fM, with the regression equation of $y = 0.0968x + 6.6899$ ($R^2 = 0.9902$), where y is the ΔE value in mV and x is the RT concentration in pg mL^{-1}. The relative standard deviation (RSD) values were between 2.8% and 10.5%. Similarly, ΔI was linearly dependent on RT concentration, within the same range, with the regression equation of ΔI (μA) = −0.3414 (RT concentration in pg mL^{-1}) − 6.9698, with a correlation coefficient

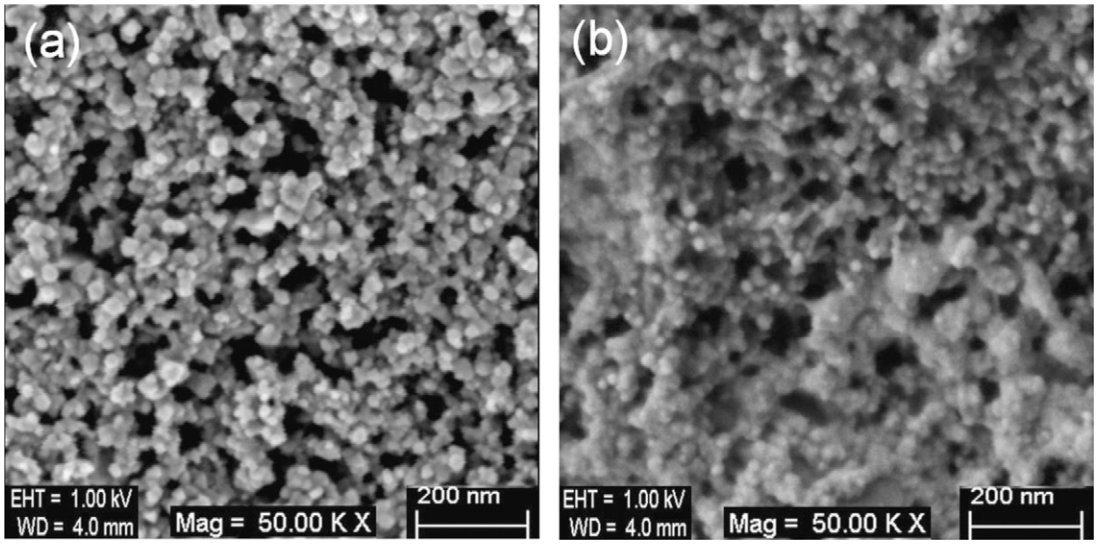

Fig. 4. Scanning electron micrographs of (a) Bare GNPs-SPCE and (b) RT-specific peptide-modified GNPs-SPCE.

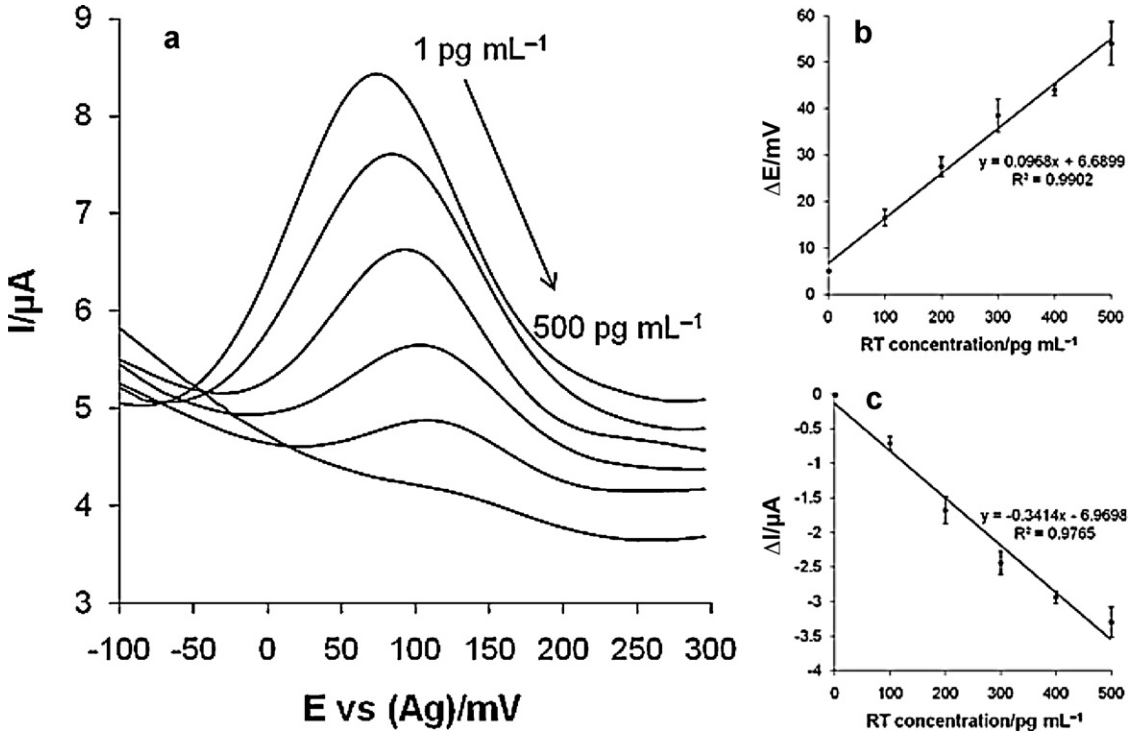

Fig. 5. (a) Square wave voltammograms at different RT concentrations: 1, 100, 200, 300, 400, and 500 pg mL^{-1}; (b) plot of potential changes (ΔE) of the redox probe *vs.* RT concentrations; (c) plot of current changes (ΔI) *vs.* RT concentrations. Error bars represent standard deviations of triplicates ($n = 3$).

of 0.9765. The RSD values ranged between 2.9% and 7.8%. At high concentrations of RT, the response became non-linear presumably indicating saturation of the biosensor surface with the target RT. The limit of detection (LOD) was 0.8 pg mL^{-1}, equivalent to 0.7 fM, estimated from 3 (S_b/m), where S_b is the standard deviation of the measurement signal for the blank and m is the slope of the linear analytical curve [34]. In order to confirm the electrochemical finding, a parallel RT analysis was performed by electrochemical impedance spectroscopy (EIS) in which the impedance of the system was evaluated as a function of increasing RT concentrations. The Nyquist plot, shown in Fig. 6, shows that the overall impedance of the system increased linearly with increasing RT concentration, which would be expected for protein binding to a surface. The RSD values ranged between 3.4% and 12.7%.

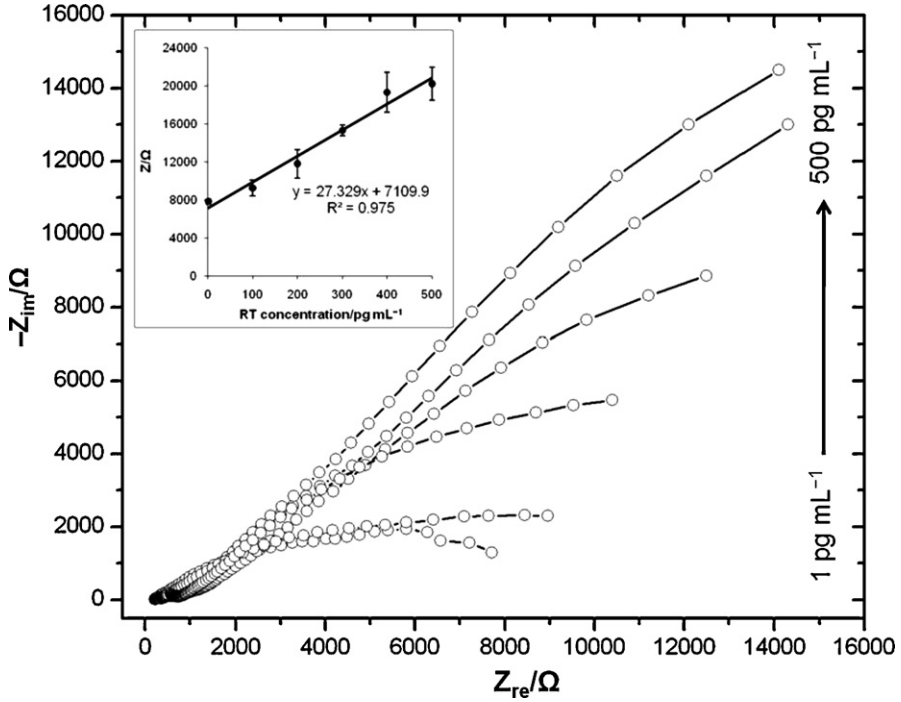

Fig. 6. Nyquist plot ($-Z_{im}$ *vs.* Z_{re}) of impedance spectra obtained at different RT concentrations (1–500 pg mL^{-1}) in 10 mM sodium phosphate buffer (pH 7.4), containing 1.0 mM $Fe(CN)_6^{3-/4-}$ as a redox probe, at a formal potential of 250 mV, frequency range from 100 kHz to 0.1 Hz, and AC amplitude of 5 mV. The upper inset shows a calibration plot of impedance *vs.* RT concentration.

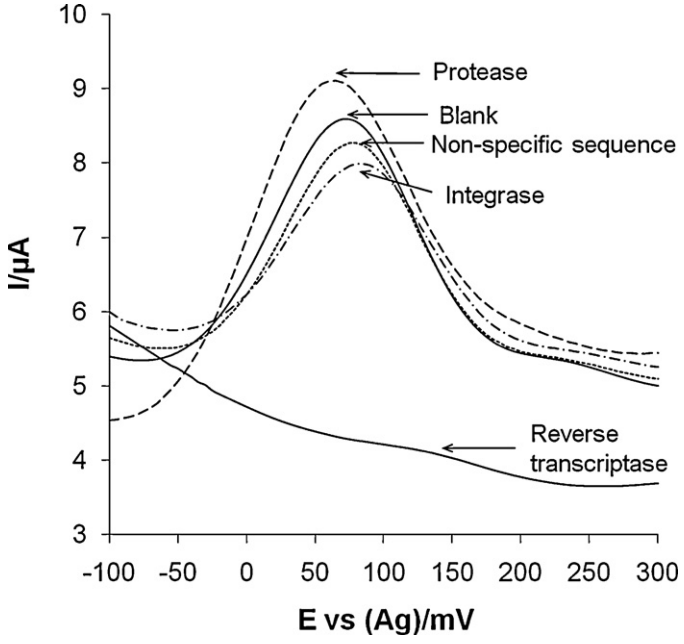

Fig. 7. Selectivity and specificity of the developed RT biosensor. SWV experiments were performed using: human serum (blank), 500 pg mL^{-1} RT, protease, and integrase using the RT-specific peptide as well as using 500 pg mL^{-1} RT with a non-specific RT peptide.

3.6. Selectivity, specificity and consistency evaluation

Selectivity experiments were performed on the other two HIV enzymes, namely protease and integrase (500 pg mL^{-1}). We were particularly concerned about potential cross-reactivity of IN due to its known interaction with the peptide sequence according to Ref [29]. However, under identical conditions (500 pg mL^{-1} enzyme added) there is a clear distinction between the response for RT and for IN (see Fig. 7). As was also pointed by one of the reviewers, the lack of the IN response is surprising and we can only speculate and attribute the observed effects to the ferrocene conjugation.

Additionally, a non-specific peptide sequence, VVStaASta (HIV-1 protease-specific), was also tested with 500 pg mL^{-1} of RT. Furthermore, the sensor specificity was assessed using the non-spiked protein-rich human serum. As shown in Fig. 7, the developed biosensor exhibited selectivity for RT binding and specificity and was able to discriminate between RT and other enzymes with minimal interference.

Furthermore, the consistency of the electrodes was evaluated, using a standard redox probe, as shown in Fig. A3 (Supplementary data). It is worth noting that the inter-electrode variation is an important factor that directly affects the precision of experimental results. This factor was assessed by measuring the relative standard deviation (RSD) of the sensor response using a standard redox probe, 1.0 mM potassium ferrocyanide in 1.0 M KCl. Thus, 6 random electrodes (a, b, c, d, e, and f) were selected from the batch received (50 electrodes) and the CV of each electrode was measured. The anodic potential of the GNPs-SPCE was -59.67 ± 1.15 mV (RSD = 1.94%) and the anodic current was 5.29 ± 0.45 μA (RSD = 8.55%). On the other hand, the cathodic potential was -181 ± 1.04 mV (RSD = 0.58%) and the cathodic current was -4.51 ± 0.37 μA (RSD = 8.25%). These results demonstrated the consistency of the GNPs-SPCEs. Noteworthy is that the results are in agreement with those recently reported by García-González et al. [69].

4. Conclusions

Overall, the results support the validity of the developed biosensor for the analysis of RT serum level and its ability to discriminate between RT and other interfering proteins at very short analysis time. Additionally, the gold nanostructured SPCE can be considered as a nanodisc array with high surface-to-volume ratio that can enhance the electrode conductivity, and improve the detection limit of the target analyte. Furthermore, the SWV technique adopted in this study is rapid, sensitive, capable of discriminating background capacitive currents, and provides a two-dimensional robust measurement of RT. Studies are currently underway with a newly developed microelectrode array that will enable a multiplexed analysis of several HIV-related proteins. This could be a significant step towards a device capable of ultrasensitive measurements of HIV enzymes and may provide a general method for studying the interactions between HIV proteins.

Acknowledgements

M. Labib is grateful to the University of Western Ontario for funding. This work was supported by grants from the Natural Sciences and Engineering Research Council of Canada (NSERC) and the Western Innovation Fund (WIF). The author is also thankful to Western Surface Science Department and Nanofabrication facility for access to their instruments and for valuable assistance.

Appendix A. Supplementary data

Supplementary data associated with this article can be found, in the online version, at doi:10.1016/j.talanta.2011.04.070.

References

[1] D.D. Richman, Nature 410 (2001) 995.
[2] B. Feng, Y. Dai, H. Zhang, L. Wang, Y. Ding, H. Zeng, Immunoassay Immunochem. 30 (2009) 457.
[3] J. Müller, Methods Mol. Biol. 630 (2010) 319.
[4] P. Brown, Nature 405 (2000) 263.
[5] C. Torti, G. Lapadula, F. Maggiolo, S. Casari, F. Suter, L. Minoli, C. Pezzoli, M.D. Pietro, G. Migliorino, E. Quiros-Roldan, N. Ladisa, L. Sighinolfi, F. Gatti, G. Carosi, HIV Clin. Trials 8 (2007) 112.
[6] M. Cavrois, C. de Noronha, W.C. Greene, Nat. Biotechnol. 20 (2002) 1151.
[7] X. Jiang, M.G. Spencer, Biosens. Bioelectron. 25 (2010) 1622.
[8] P. Swanson, C. de Mendoza, Y. Joshi, A. Golden, R.L. Hodinka, V. Soriano, S.G. Devare, J. Hackett Jr., J. Clin. Microbiol. 43 (2005) 3860.
[9] G. Stevens, N. Rekhviashvili, L.E. Scott, R. Gonin, W. Stevens, J. Clin. Microbiol. 43 (2005) 857.
[10] V. Kalia, S. Sarkar, P. Gupta, R.C. Montelaro, J. Virol. 79 (2005) 2079.
[11] M. Manocha, K.T. Chitralekha, M. Thakar, D. Shashikiran, R.S. Paranjape, D.N. Rao, Immunol. Lett. 85 (2003) 275.
[12] K.A. Mahmoud, S. Hrapovic, J.H.T. Luong, ACS Nano 2 (2008) 1051.
[13] K.A. Mahmoud, J.H.T. Luong, Anal. Chem. 80 (2008) 7056.
[14] K. Kerman, K.A. Mahmoud, H.-B. Kraatz, Chem. Commun. 37 (2007) 3829.
[15] S.G. Sarafianos, B. Marchand, K. Das, D.M. Himmel, M.A. Parniak, S.H. Hughes, E. Arnold, J. Biol. Chem. 385 (2009) 693.
[16] H. Zhang, Z. Wang, X.F. Li, X.C. Le, Angew. Chem. Int. Ed. 45 (2006) 1576.
[17] H. Zhang, X.F. Li, X.C. Le, J. Am. Chem. Soc. 134 (2008) 34.
[18] T.M.A. Gronewold, A. Baumgartner, J. Hierer, S. Sierra, M. Blind, F. Schäfer, J. Blümer, T. Tillmann, A. Kiwitz, R. Kaiser, M. Zabe-Kühn, E. Quandt, M. Famulok, J. Prot. Res. 8 (2009) 3568.
[19] J.F. Krebs, A.R. Kore, Bioconjug. Chem. 19 (2008) 185.
[20] M. Labib, P.O. Shipman, S. Martić, H.-B. Kraatz, Electrochim. Acta, 2011, in press, doi:10.1016/j.electacta.2011.03.063.
[21] M. Labib, P.O. Shipman, S. Martić, H.-B. Kraatz, Analyst 136 (2011) 708.
[22] S. Martić, M. Labib, H.-B. Kraatz, Analyst 136 (2011) 107.
[23] M. Hanif, H. Henke, S. Meier, S. Martić, M. Labib, W. Kandioller, M.A. Jakupec, V.B. Arion, H.-B. Kraatz, B.K. Keppler, C.G. Hartinger, Inorg. Chem. 49 (2010) 7953.
[24] M. Labib, M. Hedström, M. Amin, B. Mattiasson, Anal. Chim. Acta 634 (2009) 255.
[25] M. Labib, M. Hedström, M. Amin, B. Mattiasson, Anal. Bioanal. Chem. 393 (2009) 1539.
[26] M. Labib, M. Hedström, M. Amin, B. Mattiasson, Biotechnol. Bioeng. 104 (2009) 312.

[27] M. Labib, M. Hedström, M. Amin, B. Mattiasson, Anal. Chim. Acta 659 (2010) 194.
[28] M. Labib, M. Hedström, M. Amin, B. Mattiasson, Anal. Bioanal. Chem. 397 (2010) 1217.
[29] I.O. Gleenberg, A. Herschhorn, A. Hizi, J. Mol. Biol. 369 (2007) 1230.
[30] C. Fan, K.W. Plaxco, A.J. Heeger, Proc. Natl. Acad. Sci. U. S. A 100 (2003) 9134.
[31] G.K. Rowe, S.E. Creager, J. Phys. Chem. B 98 (1994) 5500.
[32] P. Zanello, Inorganic Electrochemistry, Theory, Practice and Application, Royal Society of Chemistry, 2003.
[33] E. Laviron, in: A.J. Bard (Ed.), Electroanalytical Chemistry, vol. 12, Marcel Dekker, New York, 1982, pp. 53–157.
[34] A.J. Bard, L.R. Faulkner, Electrochemical Methods: Fundamentals and Applications, Wiley, New York, 2001.
[35] E. Laviron, J. Electroanal. Chem. 101 (1979) 19.
[36] F.E. Appoh, H.-B. Kraatz, J. Phys. Chem. C 111 (2007) 4235.
[37] S. Sek, R. Moszynski, A. Sepiol, A. Misicka, R. Bilewicz, J. Electroanal. Chem. 550 (2003) 359.
[38] A.M. Belu, D.J. Graham, D.G. Castner, Biomaterials 24 (2003) 3635.
[39] H. Qi, S. Sharma, Z. Li, G.L. Snider, A.O. Orlov, C.S. Lent, T.P. Fehlner, J. Am. Chem. Soc. 125 (2003) 15250.
[40] S.K. Dey, Y.-T. Long, S. Chowdhury, T.C. Sutherland, H.S. Mandal, H.-B. Kraatz, Langmuir 23 (2007) 6475.
[41] D. Liu, G.J. Szulczewski, L.D. Kispert, A. Primak, T.A. Moore, A.L. Moore, D. Gust, J. Phys. Chem. B 106 (2002) 2933.
[42] F. Tetard, P. Djemia, M.P. Besland, P.-Y. Tessier, B. Angleraud, Thin Solid Films 482 (2005) 192.
[43] H. Darmstadt, C. Roy, Carbon 41 (2003) 2662.
[44] B. Angleraud, N. Mubumbila, P.-Y. Tessier, V. Fernandez, G. Turban, Diam. Relat. Mater. 10 (2001) 1142.
[45] F. Ghamouss, P.-Y. Tessier, A. Djouadi, M.-P. Besland, M. Boujtita, Electrochim. Acta 52 (2007) 5053.
[46] P.V. Lakshminarayanan, H. Toghiani, C.U. Pittman Jr., Carbon 42 (2004) 2433.
[47] A. Dekanski, J. Stevanović, R. Stevanović, B.Ź. Nikolić, V.M. Jovanović, Carbon 39 (2001) 1195.
[48] K.-S. Lee, M.-S. Won, H.-B. Noh, Y.-B. Shim, Biomaterials 31 (2010) 7827.
[49] F.E. Appoh, Y.-T. Long, H.-B. Kraatz, Langmuir 22 (2006) 10515.
[50] C.N.R. Rao, G.U. Kulkarni, P.J. Thomas, P.P. Edwards, Chem. Soc. Rev. 29 (2000) 27.
[51] F. Ghamouss, R. Pitson, F. Odobel, M. Boujtita, S. Caramori, C.A. Bignozzi, Electrochim. Acta 55 (2010) 6517.
[52] R.O. Kadara, N. Jenkinson, B. Li, K.H. Church, C.E. Banks, Electrochem. Commun. 10 (2008) 1517.
[53] X. Ji, C.E. Banks, A. Crossley, R.G. Compton, ChemPhysChem 7 (2006) 1337.
[54] C.E. Banks, T.J. Davies, G.G. Wildgoose, R.G. Compton, Chem. Commun. 7 (2005) 829.
[55] V. Escamilla-Gómez, D. Hernández-Santos, M.B. González-García, J.M. Pingarrón-Carrazón, A. Costa-García, Biosens. Bioelectron. 24 (2009) 2678.
[56] H. Wei, J.-J. Sun, Y. Xie, C.-G. Lin, Y.-M. Wang, W.-H. Yin, G.-N. Chen, Anal. Chim. Acta 588 (2007) 297.
[57] F. Ghamouss, E. Luais, C. Thobie-Gautier, P.-Y. Tessier, M. Boujtita, Electrochim. Acta 54 (2009) 3026.
[58] J.-C. Chen, A.S. Kumar, H.-H. Chung, S.-H. Chien, M.-C. Kuo, J.-M. Zen, Sens. Actuators B 115 (2006) 473.
[59] G. Cui, J.H. Yoo, J.S. Lee, J. Yoo, J.H. Uhm, G.S. Cha, H. Nam, Analyst 126 (2001) 1399.
[60] Y.-P. Kim, E. Oh, Y.-H. Oh, D.W. Moon, T.G. Lee, H.-S. Kim, Angew. Chem. Int. Ed. 46 (2007) 6816.
[61] R.O. Kadara, N. Jenkinson, C.E. Banks, Sens. Actuators B 138 (2009) 556.
[62] K.A. Mahmoud, J.H.T. Luong, Anal. Lett. 43 (2010) 1680.
[63] M.D. Newton, J.F. Smalley, Phys. Chem. Chem. Phys. 9 (2007) 555.
[64] F. Ricci, R.Y. Lai, K.W. Plaxco, Chem. Commun. 36 (2007) 3768.
[65] F. Ricci, R.Y. Lai, A.J. Heeger, K.W. Plaxco, J.J. Sumner, Langmuir 23 (2007) 6827.
[66] S.E. Creager, T.T. Wooster, Anal. Chem. 70 (1998) 4257.
[67] K.A. Mahmoud, H.-B. Kraatz, Chem. Eur. J. 13 (2007) 5885.
[68] J. Osteryoung, J.J. O'Dea, in: A.J. Bard (Ed.), Electroanalytical Chemistry, vol., 14, Marcel Dekker, New York, 1986, pp. 209–308.
[69] R. García-González, M.T. Fernández-Abedul, A. Pernía, A. Costa-García, Electrochim. Acta 53 (2008) 3242.